

# Interplay Between Interatomic Distance and Orbital Overlap at Control of Magnetism in $\text{FeBO}_3$ (B = Ti, Ge, Zr, Sn) Ilmenites

Renan A. P. Ribeiro, Ageo M. de Andrade, Luis H. S. Lacerda, Alexandre C. Jr. & Sergio R. de Lázaro

## Introduction

Perovskites oxides, which have the general formula  $\text{ABO}_3$ , are widely studied by theoretical or experimental means due to the large variety of intriguing properties, such as ferroelectricity, piezoelectricity, multiferroicity and others.<sup>1-3</sup> One fascinating feature for this structure is the capability to control the existence of different properties from chemical substitution and doping at A- and B-sites.<sup>4</sup> For example, the ilmenite structure based on very common mineral of earth surface ( $\text{FeTiO}_3$ ), allows a high compositional diversity of  $\text{A}^{2+}$  and  $\text{B}^{4+}$  cations that occupy alternate basal-planes along the [001] hexagonal axis of a ordered corundum structure.<sup>5</sup> The most studied ilmenite materials are Ti-based compounds with different  $\text{A}^{2+}$  (A = Mn, Fe, Ni, Co) cations, although other materials are found in this symmetry.<sup>6-9</sup> In relation to the magnetic ordering of ilmenite materials, mainly  $\text{ATiO}_3$  (A = Mn, Fe, Ni, Co), Goodenough and Stickler proved that such materials are antiferromagnetic insulators and have two different magnetic couplings constants: Intralayer ( $J_1$ ) and Interlayers ( $J_2$ ), as shown in Figure 1. For  $J_1$ , the magnetic exchange happens between A-O-A atoms and is dominated by the coupling of a  $t_{2g}$  orbital in one cation with an  $e_g$  orbital in other. Thus, the signal for exchange parameter depends upon the occupancies of the interacting orbitals making  $\text{MnTiO}_3$  antiferromagnetic and  $\text{FeTiO}_3$ ,  $\text{CoTiO}_3$ ,  $\text{NiTiO}_3$  ferromagnetic for intralayer coupling ( $J_1$ ). The  $J_2$  interactions are mediated by the  $\text{BO}_6$

clusters in the intermetallic connection A-O-B-O-A with a less contribution of a direct overlap in [001] direction due to the vacancy in cationic sublattice (Figure 1) with opposite magnetization directions between adjacent A layers (antiferromagnetic).<sup>5,10</sup>

In Fe-based ilmenite materials, aim of this study, the antiferromagnetic ordering is stabilized by the long-range exchange coupling ( $J_2$ ). Therefore,  $J_2$  is the responsible for magnetic ordering control of these materials. As previously discussed,  $J_2$  depends of intermetallic connection Fe-O-B-O-Fe suggesting that the non-magnetic B-site replacement can control the magnetism for such materials.

Other kind of materials show superexchange interactions (A-O-B-O-A) as the key for magnetic ordering control, for instance,  $\text{A}_2\text{BO}_6$  and  $\text{AA}'_3\text{B}_4\text{O}_{12}$  compounds.<sup>11</sup> Shiraki and co-workers reported that A-site ordered perovskites  $\text{CaCu}_3\text{Ge}_4\text{O}_{12}$  and  $\text{CaCu}_3\text{Sn}_4\text{O}_{12}$ , which are isostructural to antiferromagnetic  $\text{CaCu}_3\text{Ti}_4\text{O}_{12}$ , are ferromagnets.<sup>12</sup> Mizumaki and co-authors using X-ray absorption spectroscopy (XAS) for such materials proved that the antiferromagnetism in  $\text{CaCu}_3\text{Ti}_4\text{O}_{12}$  can be explained by strong hybridization of the Cu 3d, Ti 3d and O 2p orbitals, while  $\text{CaCu}_3\text{Ge}_4\text{O}_{12}$  and  $\text{CaCu}_3\text{Sn}_4\text{O}_{12}$  spectra shows hybridization only for Cu 3d and O 2p orbitals.<sup>13</sup> Similar results are found in ab initio predictions performed by Toyoda and co-workers to investigate the magnetic coupling constants of  $\text{CaCu}_3\text{B}_4\text{O}_{12}$  (B = Ti, Ge, Zr and Sn) from energetic and Density of States calculations.<sup>14</sup> Such simulations clarify the magnetic

ordering for  $\text{CaCu}_3\text{B}_4\text{O}_{12}$  materials proving that long-range superexchange interaction can turn the magnetic orientation through orbital hybridization.

From this point of view, Shimakawa and Saito synthesized solid solutions based on the mixing of non-magnetic B-cations ( $\text{B} = \text{Ge}, \text{Ti}, \text{Sn}$ ) in  $\text{CaCu}_3\text{B}_4\text{O}_{12}$  materials and shown that the magnetic orientation depends of Ti concentration in ferromagnetic  $\text{CaCu}_3\text{B}_{4-x}\text{Ti}_x\text{O}_{12}$  ( $\text{B} = \text{Ge}, \text{Sn}$ ) compounds.<sup>15</sup> In other hand, Zhu and co-author investigating  $\text{Cr}_2(\text{Te}_{1-x}\text{W}_x)\text{O}_6$  solid solutions found that magnetic interactions are controlled by tuning the orbital hybridization between Cr 3d and O 2p orbitals through W 5d. In this case the authors argue that W d and O p coupling creates a virtual hole which mediates ferromagnetic interactions between Cr atoms.<sup>16</sup> Such experimental and theoretical observations lead us to the following question: Is possible to control the magnetic ordering of Fe-based ilmenite materials by non-magnetic B-site cation replacement?

In this study, we investigate the interlayers exchange coupling of  $\text{FeBO}_3$  ( $\text{B} = \text{Ti}, \text{Ge}, \text{Zr}, \text{Sn}$ ) ilmenite materials by DFT periodic calculations. Our results proved that the orbital hybridization between B-O atoms and  $\text{Fe}^{2+}$  interlayers distances controls the magnetism of ilmenite materials making  $\text{FeTiO}_3$  and  $\text{FeGeO}_3$  antiferromagnetic, while  $\text{FeZrO}_3$  and  $\text{FeSnO}_3$  are ferromagnetic.

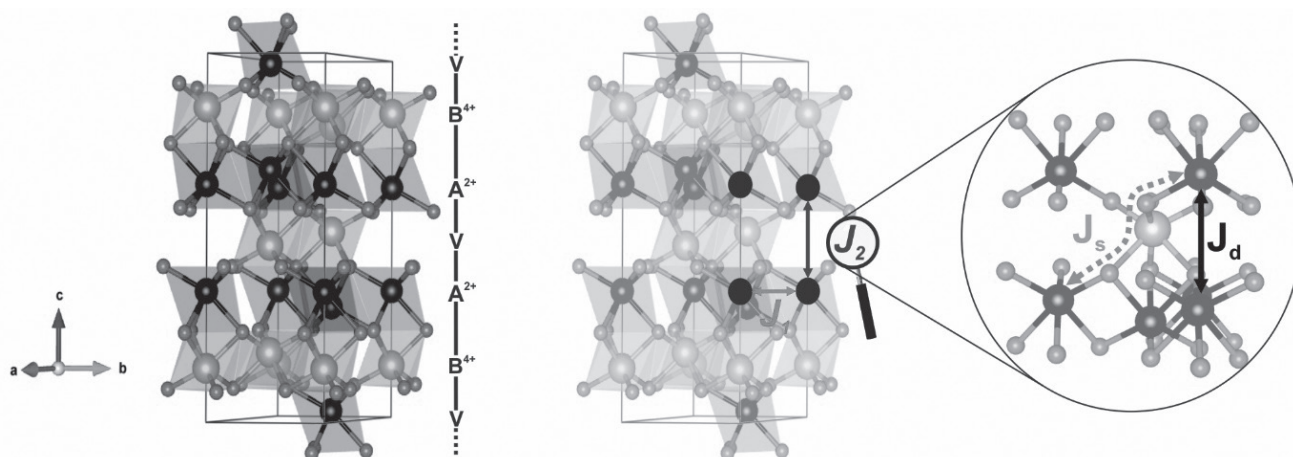


**Figure 1.** Ilmenite-type conventional unit cell and their exchange coupling constants. Black, orange and red balls represent  $\text{A}^{2+}$ ,  $\text{B}^{4+}$  and  $\text{O}^{2-}$  ions, respectively.

## Methods

Electronic and Magnetic properties of  $\text{FeBO}_3$  ( $\text{B} = \text{Ti}, \text{Ge}, \text{Zr}, \text{Sn}$ ) ilmenite materials were investigated by means of periodic DFT calculations within a hybrid functional consisting of a non-local exchange functional developed by Becke<sup>17</sup> combined with a correlation functional based on gradient of electronic density (GGA) developed by Lee, Yang and Parr<sup>18</sup>, using CRYSTAL09 code.<sup>19,20</sup> The R-3 ( $n^\circ$  148) ilmenite structure (Fig. 1) is based on experimental lattice parameters  $a = b = 5.0875 \text{ \AA}$  and  $c = 14.0827 \text{ \AA}$  and internal coordinates: Fe (0, 0, 0.3536), B (0, 0, 0.1446) and (0.3172, 0.0234, 0.2450).<sup>21</sup> All  $\text{FeBO}_3$  ( $\text{B} = \text{Ti}, \text{Ge}, \text{Zr}, \text{Sn}$ ) materials were full-relaxed (lattice parameters and atomic coordinates) in relation to system total energy of Ferromagnetic (FEM) state (Fig. 2a).

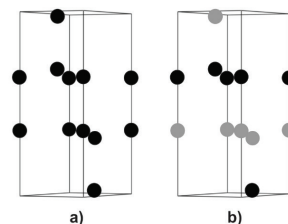


**Figure 2.** Magnetic configurations for  $\text{FeBO}_3$  ( $\text{B} = \text{Ti}, \text{Ge}, \text{Zr}, \text{Sn}$ ) ilmenite materials: a) FEM and b) AFM. The up and down-spin sites are represented by black and gray balls, respectively.

The antiferromagnetic (AFM) model (Fig. 2b) refers to the FEM optimized geometry and their energy is obtained by a single-point calculation as performed by Chartier and co-workers for  $Mn_3O_4$ .<sup>22</sup> All-electron atom-centered Gaussian-type-function (GTF) basis sets of triple-zeta valence quality, augmented by a polarization function (TZVP) are adopted for Fe, Ti, Si, Ge, Zr e O atoms,<sup>23</sup> while Sn atoms are described by pseudopotential basis set (Sn\_DURAND-21G\*); where the core electrons are described by an effective potential defined by Durand and Barthelat.<sup>24</sup> Infinite Coulomb and exchange sums are truncated by five thresholds set to  $10^{-7}$ ,  $10^{-7}$ ,  $10^{-7}$ ,  $10^{-7}$  and  $10^{-14}$ . The shrinking factor (Pack–Monkhorst and Gilat net)<sup>25</sup> was set to  $6 \times 6 \times 6$ , corresponding to 40 independent k points in the irreducible part of the Brillouin zone integration. The convergence threshold for SCF energy calculation on optimization process was set to  $10^{-8}$  Hartree.

## Results and Discussion

The optimized structural parameters of  $FeBO_3$  (B = Ti, Ge, Zr, Sn) in FEM state are presented in Table 1. The results obtained for  $FeTiO_3$  show good agreement with experimental one.<sup>21</sup> In relation to the other materials, was observed that the lattice parameters and unit cell volume were modified in accordance with the ionic radius for B-site cation. A more detailed discussion about structural properties of ilmenite materials can be found in our previous work.<sup>26</sup>

In order to analyze the magnetic properties for such materials, we used a magnetic ordering stability criteria

that was derived from comparison between the calculated total energies at FEM and AFM spin configurations. This scheme has been successfully used in a lot of theoretical studies.<sup>14,27-29</sup> In FEM configuration the spin orientation within the  $Fe^{2+}$  layers and in adjacent layers is parallel (Fig. 2a); whereas, for AFM state the  $Fe^{2+}$  magnetic moments are ferromagnetic coupled in a [001] plane but, they have opposite orientation for adjacent layers in c axis (Fig. 2b). The energy results indicate that  $FeTiO_3$  and  $FeGeO_3$  are AFM materials, while  $FeZrO_3$  and  $FeSnO_3$  are FEM. In the following subsections, we will discuss the interlayers magnetic ordering for  $FeBO_3$  ilmenite materials considering the existence of both direct ( $J_d$ ) and superexchange ( $J_s$ ) couplings between adjacent  $Fe^{2+}$  layers, as shown in Figure 1.

As previously discussed, the ilmenite structure arrangement enables a vacancy formation between adjacent  $Fe^{2+}$  layers separated by a B-site plane. From this, the interlayer magnetic coupling integral can be visualized as a direct coupling between 3d orbitals of adjacent  $Fe^{2+}$  cations. Once the vacancy formation occurs in cationic (B) sublattice and the direct exchange coupling depends on the distance, the non-magnetic B-site cation modification can affect the magnetic ordering in such direction. To investigate such hypothesis, the energy difference ( $\Delta E$ ) between FEM and AFM states was plotted against the interatomic distance for  $Fe^{2+}$  layers, as shown in Figure 3. From these results, it was observed that the FEM state is stabilized for ilmenite materials with large B-site metals (Sn, Zr), whereas, contracted ilmenite cells (Ge, Ti) exhibit an AFM behavior.

**Table 1.** Theoretical and Experimental results for structural parameters and Energy Difference ( $\Delta E$ ) between magnetic configurations for  $FeBO_3$  (B = Ti, Ge, Zr, Sn) ilmenite materials.

Models	Lattice Parameters (Å)		Bond distance (Å)				Fe-Fe (Å)	$\Phi$ O-B-O (degrees)	$\Delta E$ (meV)
			Fe-Oax	Fe-Oeq	B-Oax	B-Oeq			
FeTiO3	5.093	14.226	2.180	2.100	2.120	1.860	4.158	160.43	-45.8
FeGeO3	4.762	14.191	2.243	2.075	1.978	1.882	4.056	165.00	-17.0
FeZrO3	5.453	14.242	2.216	2.152	2.223	2.057	4.193	161.50	63.3
FeSnO3	5.275	14.437	2.263	2.139	2.162	2.046	4.111	166.81	94.8
Exp.21	5.087	14.083	2.200	2.080	2.090	1.870	-	-	-

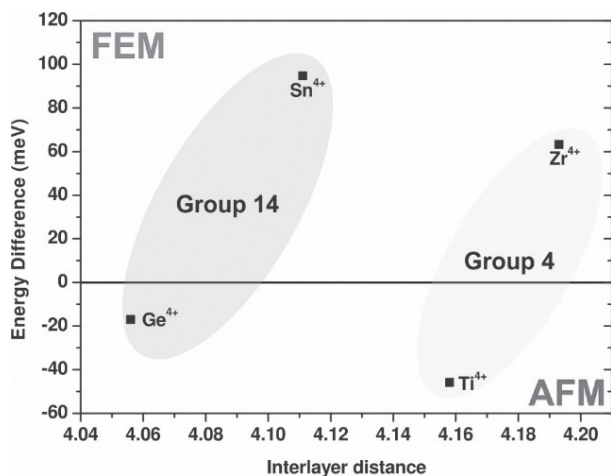


**Figure 3.** Energy difference (in meV) between AFM and FEM configuration as function of Fe-Fe interlayer distance (in Å).

This result can be discussed as function of electronic repulsion between  $\text{Fe}^{2+}$  atoms 3d orbitals in different layers, as presented in Figure 4. In this case, we use the c-axis oriented 3d orbital ( $3d_{z^2}$ ), once the cationic vacancy induces a coupling in such direction. In Figure 4 is possible to see that B-cation volume control the distance between different  $\text{Fe}^{2+}$  layers in accordance with the results presented in Table 1 and Figure 3. For instance, from periodic Group 14 (Sn, Ge), the increase in B-site cation ionic radius (Ge = 0.53 Å; Sn = 0.69 Å) induces an angular distortion in O-B-O bonds in axial plane, which causes an increase in bond distances allowing a bigger spacing between  $\text{Fe}^{2+}$  layers (Table 1). The same behavior was observed when we compare the  $\text{FeBO}_3$  (B=Ti, Zr) ilmenite materials from periodic Group 4 (Table 1 and Figure 3).

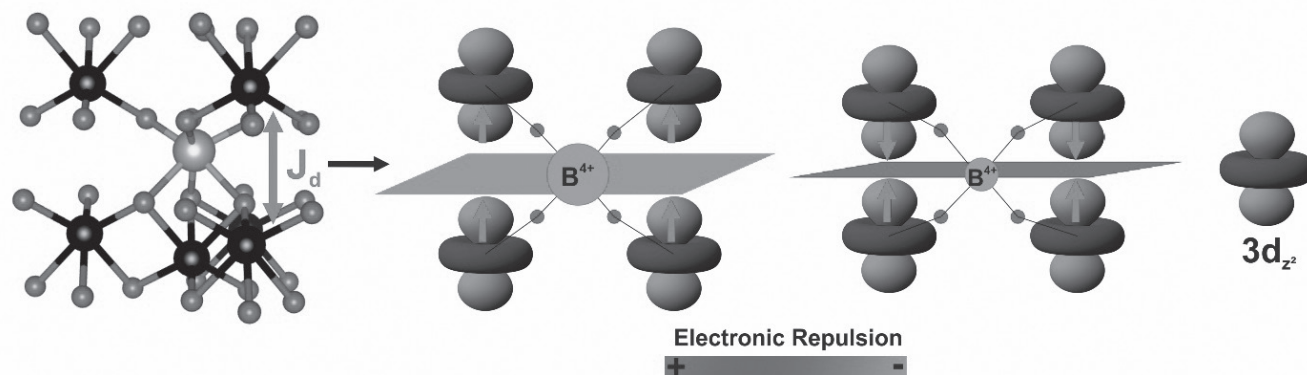


**Figure 4.** Representation of electronic repulsion between adjacent  $\text{Fe}^{2+}$  layer in  $\text{FeBO}_3$  (B = Ti, Ge, Zr, Sn) as function of ionic radius of B-site cation and its influence on magnetic ordering.

In these different periodic Groups (4 and 14), such O-B-O angular distortion induces a decrease of direct overlap between  $3d_{z^2}$  orbitals from different layers enabling a FEM ground-state due to the control of smaller electronic repulsion between the unpaired electrons. On the other hand, for smaller cations the proximity between  $\text{Fe}^{2+}$  layers increase the overlap between  $3d_{z^2}$  orbitals stabilizing an AFM ground-state, once the higher electronic repulsion induces a pairing of electrons in agreement with the Pauli Exclusion Principle.

Regarding the results presented in Figure 3, was noted that the last discussion is not valid if we compare B-site cation from different periodic groups. For instance, the expected result for  $\text{FeTiO}_3$  (Group 4) from the interlayer distance (Figure 3) suggests a FEM ordering due to the larger spacing in comparison to the  $\text{FeSnO}_3$  material (Group 14), which can be attributed to the chemical differences between such metals, for instance, valence orbitals, ionization potential, ionic radius and others.

As previously cited in the introduction section is know that the B-site cations for ilmenite materials enables a connection between different  $\text{Fe}^{2+}$  layers, which is denominated intermetallic connection Fe-O-B-O-Fe. Goodenough and Stickler argue that this kind of interaction originates a long-range coupling, which is the most fundamental reason to the AFM arrangement observed in ilmenite materials.<sup>5</sup> However, this kind of long-range coupling is also observed in other materials that exhibit variations of the magnetic ordering as function of valence orbitals from “atom-bridge”.<sup>12-14</sup>

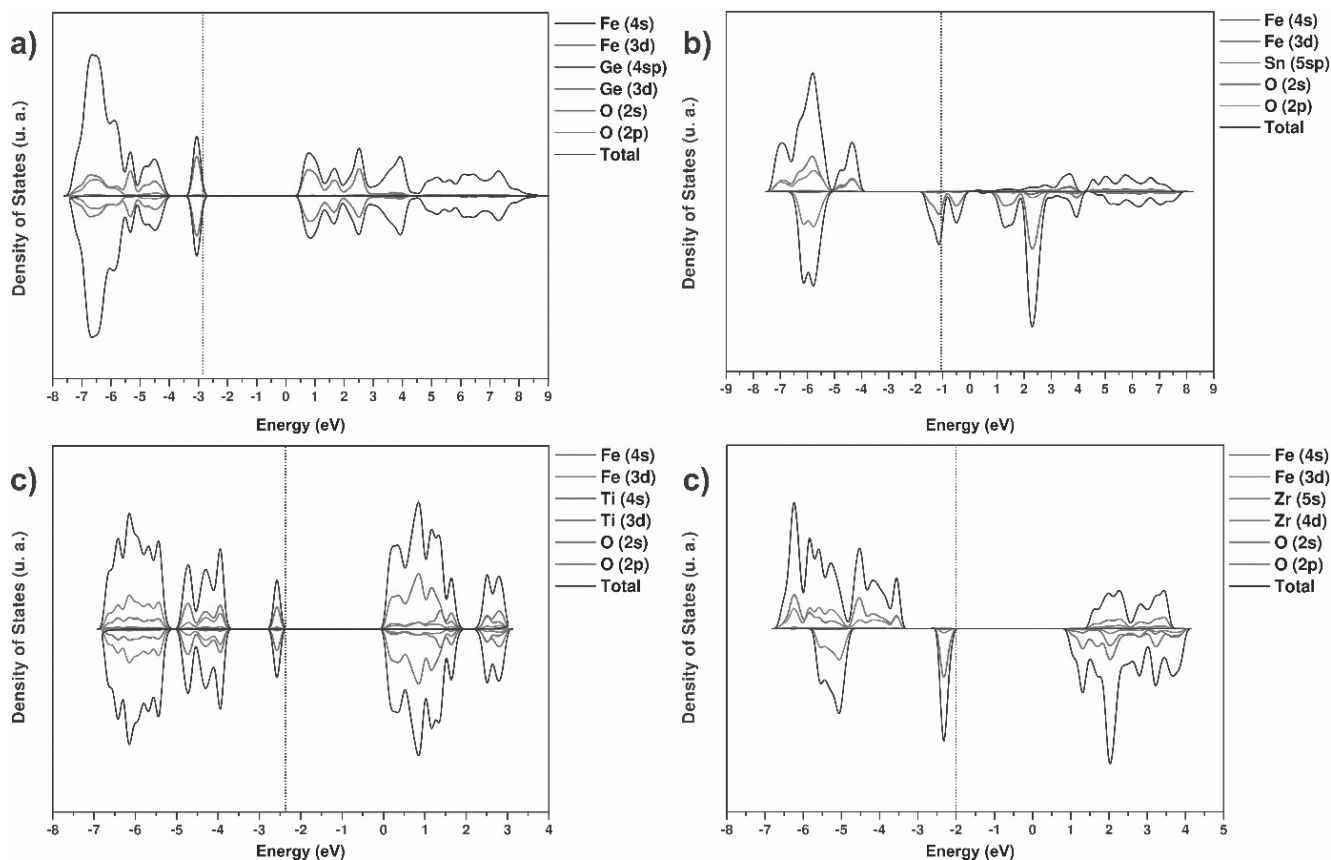


**Figure 5.** Spin-polarized Density of States for a) FeGeO<sub>3</sub>, b) FeSnO<sub>3</sub>, c) FeTiO<sub>3</sub>, d) FeZrO<sub>3</sub> ilmenite materials

In order to investigate the orbital overlap effect on magnetic ordering of ilmenite materials, the spin-polarized Density of States was evaluated as presented in Figure 5. From this result is clearly shown that the Valence Band (VB) exhibits the same pattern of orbitals distribution for all investigated ilmenite materials: Fe 3d orbitals are always overlapped with O 2p orbitals in VB. However, for Conduction Band (CB) were observed different compositions as function of valence orbitals from B-site metals. For FeGeO<sub>3</sub> and FeSnO<sub>3</sub> materials (Figure 5a, b), the CB is mainly composed by 4sp and 5sp of the Ge and Sn atoms, respectively; whereas, for FeTiO<sub>3</sub> and FeZrO<sub>3</sub> the 3d and 4d orbitals of the Ti and Zr atoms are superposed with O 2p orbitals, respectively (Figure 5a, b).

Following the same discussion addressed by Toyoda and co-workers for CaCu<sub>3</sub>B<sub>4</sub>O<sub>12</sub> (B = Ti, Ge, Zr, Sn) materials, the expected behavior suggest a FEM ordering for B-site cations without d valence orbitals; whereas, the AFM ground state is stabilized for transitions metals from d valence orbitals. Such expected result can be related to the large overlap between d and 2p oxygen orbitals, which strengthen the intermetallic connection and, consequently, induces a large electronic repulsion among unpaired electrons stabilizing the AFM configuration from Pauli Exclusion Principle.<sup>13,14</sup> However, the comparison between the ground-states for FeTiO<sub>3</sub> and FeZrO<sub>3</sub> materials indicates that only Ti-based ilmenite (Figure 5c) has an AFM ordering, while FeZrO<sub>3</sub> (Figure 5d) is a FEM semiconductor. This result can be attributed to the contribution of d valence orbitals in CB observed from

DOS results. For  $\text{FeTiO}_3$  (Figure 5c), a large contribution of 3d overlapped with O 2p orbital was observed between 0 to 2 eV suggesting a bigger overlap between these states providing strengthens in intermetallic connection. On the other hand, the smaller overlap between Zr(4d) and O(2p) orbitals added large Zr-O bond distances enabling a smaller interlayer electronic repulsion, which is responsible by FEM ordering.

Similarly, the  $\text{FeBO}_3$  (B=Ge, Sn) ilmenite materials are expected to be FEM due to the absence of d valence orbitals (Figure 5a, b). However, only Sn-based ilmenite has this configuration suggesting a large effect of ionic radius and interlayer distance of the  $\text{FeO}_6$  clusters. Comparing the ionic radius and bond distance for  $\text{FeBO}_3$  (B=Ge, Sn) materials was observed that the increase in ionic radius from  $\text{Ge}^{4+}$  to  $\text{Sn}^{4+}$  induces a large spacing among  $\text{Fe}^{2+}$  layers in intermetallic connection that drastically reduce the electronic repulsion and stabilize the FEM configuration. The summation of these theoretical results demonstrates that the magnetic ordering of ilmenite materials can be controlled from a complex relation between ionic radius and valence orbitals of non-magnetic metals occupying B-site.

## Conclusions

From theoretical results obtained through DFT/B3LYP theory applied to the ilmenite structure of  $\text{FeBO}_3$  (B = Ti, Ge, Zr, Sn) materials, it was observed that structural parameters were calculated with good agreement to experimental results and describe very well the B-site effect on such parameters. Furthermore, the simulations performed in this work reveal the effect of non-magnetic B-site cations at control of magnetic ordering of ilmenite materials from a complex relation between interlayer distance, valence orbital and intermetallic connection. In particular,  $\text{FeSnO}_3$  and  $\text{FeZrO}_3$  materials exhibit ferromagnetic ground state due to the large spacing among  $\text{Fe}^{2+}$  layers and the weak intermetallic connections; whereas,  $\text{FeGeO}_3$  and  $\text{FeTiO}_3$  materials are antiferromagnetic for the opposite reasons.

## Acknowledgments

The authors are grateful for the support given from the CAPES, UEPG and Fundação Araucária.

## References

- Bhalla, A. S.; Guo, R. Y.; Roy, R. *Materials Research Innovations*, 4, 3, (2000).
- Wu, H.; Li, L.; Liang, L.-Z.; Liang, S.; Zhu, Y.-Y.; Zhu, X.-H. *Journal of the European Ceramic Society*, 35, 411, (2015).
- Zhu, X. *Recent Patents on Nanotechnology*, 3, 42, (2009).
- King, G.; Woodward, P. M. *Journal of Materials Chemistry*, 20, 5785, (2010).
- Goodenough, J. B. *Physical Review B*, 164, 768, (1967).
- Abrahams, S. C. *Acta Crystallographica Section B-Structural Science*, 63, 257, (2007).
- Gou, H.; Zhang, J.; Li, Z.; Wang, G.; Gao, F.; Ewing, R. C.; Lian, J. *Applied Physics Letters*, 98, (2011).
- Okada, T.; Narita, T.; Nagai, T.; Yamanaka, T. *American Mineralogist*, 93, 39, (2008).
- Zhang, T. S.; Shen, Y. S.; Zhang, R. F. *Materials Letters*, 23, 69, (1995).
- Kato, H.; Yamada, M.; Yamauchi, H.; Hiroyoshi, H.; Takei, H.; Watanabe, H. *Journal of the Physical Society of Japan*, 51, 1769, (1982).
- Shimakawa, Y.; Mizumaki, M. *Journal of Physics-Condensed Matter*, 26, (2014).
- Shiraki, H.; Saito, T.; Yamada, T.; Tsujimoto, M.; Azuma, M.; Kurata, H.; Isoda, S.; Takano, M.; Shimakawa, Y. *Physical Review B*, 76, (2007).
- Mizumaki, M.; Saito, T.; Shiraki, H.; Shimakawa, Y. *Inorganic Chemistry*, 48, 3499, (2009).
- Toyoda, M.; Yamauchi, K.; Oguchi, T. *Physical Review B*, 87, (2013).
- Shimakawa, Y.; Saito, T. *Physica Status Solidi B-Basic Solid State Physics*, 249, 423, (2012).
- Zhu, M.; Do, D.; Dela Cruz, C. R.; Dun, Z.; Zhou, H. D.; Mahanti, S. D.; Ke, X. *Physical Review Letters*, 113, (2014).
- Becke, A. D. *J. Chem. Phys.*, 98, 5648, (1993).
- Lee, C.; Yang, W.; Parr, R. G. *Physical Review B*, 37, 785, (1988).
- Dovesi, R.; Orlando, R.; Civalleri, B.; Roetti, C.; Saunders, V. R.; Zicovich-Wilson, C. M. *Z. Kristallogr*, 220, 571, (2005).
- Dovesi, R.; Saunders, V. R.; Roetti, C.; Orlando, R.; Zicovich-Wilson, C. M.; Pascale, F.; Civalleri, B.; Doll, K.; Harrison, N. M.; Bush, I. J.; D'Arco, P.; Llunell, M. *CRYSTAL09 User's Manual*; University of Torino: Torino, 2009.
- Wechsler, B. A.; Prewitt, C. T. *American Mineralogist*, 69, 176, (1984).
- Chartier, A.; D'Arco, P.; Dovesi, R.; Saunders, V. R. *Physical Review B*, 60, 14042, (1999).

23. Peintinger, M. F.; Oliveira, D. V.; Bredow, T. J. *Comput. Chem.*, 34, 451, (2013).
  24. Durand, P.; Barthelat, J.-C. *Theoret. Chim. Acta*, 38, 283, (1975).
  25. Monkhorst, H. J.; Pack, J. D. *Physical Review B*, 13, 5188, (1976).
  26. Ribeiro, R. A. P.; de Lazaro, S. R. *Rsc Advances*, 4, 59839, (2014).
  27. Lebernegg, S.; Schmitt, M.; Tsirlin, A. A.; Janson, O.; Rosner, H. *Physical Review B*, 87, (2013).
  28. Liu, Y. P.; Fuh, H. R.; Wang, Y. K. *Computational Materials Science*, 92, 63, (2014).
  29. Liu, M.; Lv, Z.-L.; Cheng, Y.; Ji, G.-F.; Gong, M. *Computational Materials Science*, 79, 811, (2013).
- 

Renan A. P. Ribeiro<sup>a\*</sup>, Ageo  
Meier de Andrade<sup>a</sup>, Luis H.  
S. Lacerda<sup>a</sup>, Alexandre C.  
Jr.<sup>b</sup> & Sergio R. de Lázaro<sup>a</sup>

<sup>a</sup> Department of Chemistry, State University of Ponta Grossa, Av. General Carlos Cavalcanti, 4748, 84030-900, Ponta Grossa, PR, Brazil

<sup>b</sup> Department of Physics, State University of Ponta Grossa, Av. General Carlos Cavalcanti, 4748, 84030-900, Ponta Grossa, PR, Brazil

\*E-mail: ribeiroapr@gmail.com